Published in final edited form as:
Cell. 2014 January 16; 156(0): 170–182. doi:10.1016/j.cell.2013.11.047.

Potentiated Hsp104 variants antagonize diverse proteotoxic misfolding events

Meredith E. Jackrel[1], **Morgan E. DeSantis**[1,2], **Bryan A. Martinez**[3], **Laura M. Castellano**[1,4], **Rachel M. Stewart**[1], **Kim A. Caldwell**[3], **Guy A. Caldwell**[3], and **James Shorter**[1,2,4,*]

[1]Department of Biochemistry and Biophysics, Perelman School of Medicine at the University of Pennsylvania, Philadelphia, PA 19104, U.S.A.

[2]Department of Biochemistry and Molecular Biophysics Graduate Group, Perelman School of Medicine at the University of Pennsylvania, Philadelphia, PA 19104, U.S.A.

[3]Department of Biological Sciences, University of Alabama, Tuscaloosa, AL 35487, U.S.A.

[4]Department of Pharmacology Graduate Group, Perelman School of Medicine at the University of Pennsylvania, Philadelphia, PA 19104, U.S.A.

Summary

There are no therapies that reverse the proteotoxic misfolding events that underpin fatal neurodegenerative diseases including amyotrophic lateral sclerosis (ALS) and Parkinson disease (PD). Hsp104, a conserved hexameric AAA+ protein from yeast, solubilizes disordered aggregates and amyloid, but has no metazoan homologue and only limited activity against human neurodegenerative disease proteins. Here, we reprogram Hsp104 to rescue TDP-43, FUS, and α-synuclein proteotoxicity by mutating single residues in helix 1, 2, or 3 of the middle domain or the small domain of nucleotide-binding domain 1. Potentiated Hsp104 variants enhance aggregate dissolution, restore proper protein localization, suppress proteotoxicity, and in a *C. elegans* PD model attenuate dopaminergic neurodegeneration. Potentiating mutations reconfigure how Hsp 104 subunits collaborate, desensitize Hsp104 to inhibition, obviate any requirement for Hsp70, and enhance ATPase, translocation, and unfoldase activity. Our work establishes that disease-associated aggregates and amyloid are tractable targets and that enhanced disaggregases can restore proteostasis and mitigate neurodegeneration.

Introduction

Protein misfolding underpins several fatal neurodegenerative disorders including amyotrophic lateral sclerosis (ALS) and Parkinson disease (PD) (Cushman et al., 2010). In PD, α-synuclein (α-syn) forms highly toxic pre-fibrillar oligomers and amyloid fibrils that accumulate in cytoplasmic Lewy bodies (Cushman et al., 2010). In ALS, TDP-43 or FUS accumulate in cytoplasmic inclusions in degenerating motor neurons (Robberecht and Philips, 2013). Unfortunately, treatments for these disorders are palliative and ineffective due to the apparent intractability of aggregated proteins. Effective therapies are urgently

*Correspondence: jshorter@mail.med.upenn.edu.

needed that eliminate the causative proteotoxic misfolded conformers via degradation or reactivation of the proteins to their native fold.

Inspiration can be drawn from nature where amyloidogenesis and protein misfolding have been subjugated for adaptive modalities (Newby and Lindquist, 2013). For example, beneficial yeast prions are tightly regulated by Hsp104, a hexameric AAA+ protein, which rapidly deconstructs various amyloids and pre-fibrillar oligomers (DeSantis et al., 2012; Lo Bianco et al., 2008; Newby and Lindquist, 2013). Hsp104 also reactivates proteins from disordered aggregates after environmental stress (Shorter, 2008). Hsp104 is highly conserved in eubacteria and eukaryotes except for metazoa, which bafflingly lack an Hsp104 homologue and display limited ability to disaggregate disordered and amyloid aggregates (Duennwald et al., 2012; Shorter, 2008, 2011). Thus, Hsp104 could be harnessed to augment human proteostasis and counter protein misfolding in neurodegenerative disease (Shorter, 2008). Indeed, Hsp104 synergizes with human Hsp70 and Hsp40 to resolve various misfolded species linked with human neurodegenerative disease and can partially antagonize protein misfolding and neurodegeneration in metazoa (Cushman-Nick et al., 2013; DeSantis et al., 2012; Duennwald et al., 2012; Lo Bianco et al., 2008; Shorter, 2011; Vacher et al., 2005). Hsp70 overexpression can also mitigate neurodegeneration (Cushman-Nick et al., 2013). However, these potentially therapeutic activities remain limited and vast improvements are needed to maximize therapeutic potential. Indeed, very high concentrations of Hsp104 are needed to antagonize human neurodegenerative disease proteins, which Hsp104 never ordinarily encounters, and some substrates are refractory to Hsp104 (DeSantis et al., 2012; Lo Bianco et al., 2008).

A key but elusive goal is to engineer or evolve optimized chaperones against neurodegenerative disease substrates to maximize therapeutic efficacy (Shorter, 2008). Chaperones are impractical targets for protein engineering due to their typically large size, and protein disaggregases such as Hsp104 have poorly understood structures, making rational design challenging (Saibil, 2013). Here, we broach this issue and isolate potentiated Hsp104 variants that eradicate TDP-43, FUS, and α-syn aggregates and potently suppress toxicity. We report the first artificially engineered chaperones to optimize proteostasis and thwart neurodegeneration. We suggest that neuroprotection may be possible for diverse neurodegenerative diseases via subtle structural modifications of existing chaperones.

Results

Substrate-binding tyrosines in Hsp104 pore loops are optimal for disaggregation

Hsp104 is adapted for disaggregation of the yeast proteome. We sought to engineer Hsp104 variants to disaggregate TDP-43, an RNA-binding protein with a prion-like domain (Cushman et al., 2010), which has no yeast homologue and is not a natural Hsp104 substrate. A yeast model of TDP-43 proteinopathies has been developed in which TDP-43 is overexpressed via a galactose-inducible promoter (Johnson et al., 2008). TDP-43 aggregates in the cytoplasm and is toxic to yeast, which phenocopies TDP-43 pathology in disease and has enabled identification of common ALS genetic risk factors (Elden et al., 2010). To explore Hsp104 sequence space against TDP-43 toxicity we employed Δ*hsp104* yeast to assess Hsp104 variants in the absence of wild-type (WT) Hsp104. TDP-43 is highly toxic in Δ*hsp104* yeast and $Hsp104^{WT}$ provides minimal rescue of toxicity (Johnson et al., 2008). Thus, Δ*hsp104* yeast provide a platform to isolate more active Hsp104 variants. Each Hsp104 monomer contains two nucleotide binding domains (NBD1 and NBD2), as well as an N-terminal, middle, and C-terminal domain (DeSantis and Shorter, 2012). Hsp104 forms ring-shaped hexamers with a central pore through which substrate is threaded. To alter substrate specificity we assessed Hsp104 variants bearing mutations in Hsp104's two substrate-binding pore loops (DeSantis and Shorter, 2012). We mutated the conserved pore

loop residues, Y257 and Y662, which mediate substrate binding and translocation (Tessarz et al., 2008) to all amino acids and screened this library of 400 variants for rescue of TDP-43 toxicity. After several rounds of selection, nearly all the variants possessed Y at one, or more often, both pore-loop positions. None of the pore-loop Hsp104 variants were more active than $Hsp104^{WT}$ in rescuing TDP-43 toxicity. Thus, Y257 and Y662 are likely optimal for disaggregation.

Select missense mutations in the middle domain potentiate Hsp104 activity

Next, we explored the coiled-coil middle domain (MD) of Hsp104, which is less conserved than the substrate-binding pore loops. MD variants can have unexpected gain of function phenotypes (Schirmer et al., 2004). The Hsp104 MD (residues 411–538; Fig. 1A) facilitates: optimal ATPase activity, communication between NBD1 and NBD2, intrinsic disaggregase activity, and interactions with Hsp70 during disordered aggregate dissolution (DeSantis and Shorter, 2012). We randomly mutagenized the MD and screened this Hsp104 library against α-syn, FUS, or TDP-43 toxicity (Johnson et al., 2008; Outeiro and Lindquist, 2003; Sun et al., 2011). We employed Δ*hsp104* yeast, as deletion of Hsp104 does not affect α-syn, FUS, or TDP-43 toxicity (Johnson et al., 2008; Ju et al., 2011). We identified several Hsp104 variants that potently rescued α-syn, FUS, and TDP-43 toxicity, whereas $Hsp104^{WT}$ was ineffective (Fig. 1B). Potentiated Hsp104 variants had a missense mutation in helix 1 ($Hsp104^{V426L}$), or in the distal loop between helix 1 and 2 ($Hsp104^{A437W}$), or in helix 3 ($Hsp104^{A503V}$ or $Hsp104^{Y507C}$) (Fig. 1A, B). Unexpectedly, we uncovered an enhanced variant with a missense mutation in the NBD1 small domain ($Hsp104^{N539K}$) (Fig. 1A, B). Thus, the MD or small domain of NBD1 can be mutated to potentiate Hsp104 activity against α-syn, FUS, and TDP-43.

Two potentiating mutations: A503V and Y507C lie in MD helix 3. Thus, we performed a valine scan of helix 3 (residues 498–507) in search of additional enhanced variants (Fig. 1C, D). Most helix-3 valine substitutions behaved like $Hsp104^{WT}$ (Fig. 1C). However, $Hsp104^{D504V}$ suppressed α-syn, FUS, and TDP-43 toxicity (Fig. 1C). $Hsp104^{D498V}$ and $Hsp104^{Y507V}$ suppressed FUS and α-syn toxicity, but not TDP-43 toxicity (Fig. 1C). Thus, select missense mutations in helix 3 engender potentiated Hsp104 variants with altered substrate specificity.

Two different Y507 mutations yielded enhanced variants. Thus, we explored other substitutions at this position. $Hsp104^{Y507A}$, $Hsp104^{Y507C}$, and $Hsp104^{Y507D}$ rescued α-syn, FUS, and TDP-43 toxicity (Fig. S1). Likewise, additional substitutions at D504 (to C), V426 (to G), or N539 (to E, D, G, or K) yielded potentiated Hsp104 variants against FUS toxicity (Fig. S1). Thus, diverse mutations at specific positions in the MD enhance Hsp104 activity.

$Hsp104^{A503X}$ variants suppress TDP-43 toxicity and promote its proper localization

$Hsp104^{A503V}$ was among the strongest suppressors of α-syn, FUS, and TDP-43 toxicity, and so we explored this position further and mutated A503 to all amino acids. None of these Hsp104 variants were toxic to yeast when overexpressed at 30°C (Fig. S2). Mutation of A503 to V, S, or C suppressed TDP-43 toxicity: $Hsp104^{A503C}$ most strongly suppressed TDP-43 toxicity, followed by $Hsp104^{A503S}$ and $Hsp104^{A503V}$ (Fig. 2A, B, S3A). Surprisingly, mutation of A503 to nearly any residue suppressed TDP-43 toxicity, whereas $Hsp104^{A503P}$ enhanced toxicity (Fig. 2A, S3A). Indeed, we could now mutate the conserved pore loop Y residues (Y257 and Y662) to F ($Hsp104^{A503V\text{-}DPLF}$) and retain suppression of TDP-43 toxicity (Fig. 2A). Rescue of TDP-3 toxicity was not due to lower levels of TDP-43, which was roughly equal across strains (Fig. 2C). Likewise, rescue could not be explained by higher Hsp104 expression. Hsp104 variants were expressed at slightly lower

levels than Hsp104^{WT} (Fig. 2C). Quantitative immunoblot revealed that Hsp104 hexamer:TDP-43 ratios were ~1:1.31 for Hsp104^{WT} and ~1:2.20 for Hsp104^{A503V}.

Hsp70 and Hsp26 levels were also similar for all strains, indicating that Hsp104 variants do not induce a heat shock response (HSR; Fig. 2C). Hsp104^{A503V} expression from the native Hsp104 promoter (which is weaker than the galactose promoter) suppressed TDP-43 toxicity (Fig. S4A, B). Here, quantitative immunoblot revealed that Hsp104 hexamer:TDP-43 ratios were ~1:1.70 for Hsp104^{WT} and ~1:4.55 for Hsp104^{A503V}. Thus, even low Hsp104^{A503V} levels rescued TDP-43 toxicity. Finally, Hsp104^{A503V}, Hsp104^{A503S}, and Hsp104$^{A503V\text{-}DPLF}$ rescued TDP-43 toxicity in Δ*ire1* (to disrupt the unfolded protein response [UPR]) and Δ*atg8* (to disrupt autophagy) strains (Fig. 2D). Thus, neither the UPR nor autophagy, are needed for enhanced Hsp104 variants to rescue TDP-43 toxicity.

TDP-43 normally shuttles between the nucleus and cytoplasm. However, in ALS, TDP-43 is usually depleted from the nucleus and aggregated in the cytoplasm (Robberecht and Philips, 2013). Indeed, cytoplasmic TDP-43 aggregates persist upon Hsp104^{WT} overexpression (Fig. 2E). By contrast, Hsp104^{A503V} eliminated cytoplasmic TDP-43 aggregates and ~46% of cells had nuclear TDP-43 localization (Fig. 2E). Accordingly, Hsp104^{A503V} reduced the amount of insoluble TDP-43 by ~57%, whereas Hsp104^{WT} was ineffective (Fig. 2F). Thus, Hsp104^{A503V} eliminates TDP-43 aggregation and toxicity and restores TDP-43 to the nucleus. These phenotypes are a therapeutic goal for ALS and other TDP-43 proteinopathies. Several suppressors of TDP-43 toxicity have been isolated in yeast, but none clear cytoplasmic TDP-43 aggregates (Sun et al., 2011). Thus, our enhanced Hsp104 variants are the first genetic suppressors that eradicate TDP-43 aggregates and restore TDP-43 to the nucleus.

Hsp104^{A503X} variants suppress FUS toxicity and aggregation

Next, we tested Hsp104^{A503X} variants for rescue of FUS toxicity in yeast. FUS, like TDP-43 is a nuclear RNA-binding protein with a prion-like domain that forms cytoplasmic aggregates in degenerating neurons of FUS proteinopathy patients and in yeast (Ju et al., 2011; Robberecht and Philips, 2013; Sun et al., 2011). As for TDP-43, mutation of A503 to any amino acid except P strongly suppressed FUS toxicity, as did Hsp104$^{A503V\text{-}DPLF}$ (Fig. 3A, B, S3B). Hsp104^{A503G} most strongly suppressed FUS toxicity (Fig. 3A, B, S3B). Rescue of FUS toxicity by Hsp104^{A503X} variants (or Hsp104^{D498V} or Hsp104^{D504V}) could not be explained by: lower FUS levels, induction of Hsp70 or Hsp26 in a HSR, or higher Hsp104 levels (Fig. 3C). Indeed, quantitative immunoblot revealed that Hsp104 hexamer:FUS ratios were ~1:5.13 for Hsp104^{WT} and ~1:3.25 for Hsp104^{A503V}. Even low Hsp104^{A503V} levels expressed from the natural Hsp104 promoter suppressed FUS toxicity (Fig. S4C, D). Here, quantitative immunoblot revealed that Hsp104 hexamer:FUS ratios were ~1:5.21 for Hsp104^{WT} and ~1:9.58 for Hsp104^{A503V}. Rescue of FUS toxicity by Hsp104^{A503V}, Hsp104^{A503S}, and Hsp104$^{A503V\text{-}DPLF}$ occurred in Δ*ire1* strains and Δ*atg8* strains (Fig. 3D). Thus, the UPR and autophagy are not required for potentiated Hsp104 variants to suppress FUS toxicity.

Hsp104^{A503V} eliminated FUS aggregates, whereas Hsp104^{WT} had no effect (Fig. 3E). In contrast to TDP-43, FUS was now diffuse in the cytoplasm (Fig. 3E) because the yeast nuclear transport machinery fails to decode the FUS PY-NLS (Ju et al., 2011). Hsp104^{A503V} reduced the amount of insoluble FUS by ~49%, whereas Hsp104^{WT} was ineffective (Fig. 3F). Genome-wide overexpression screens have yielded several suppressors of FUS toxicity in yeast, but none that solubilize FUS inclusions (Ju et al., 2011; Sun et al., 2011). Thus, potentiated Hsp104 variants are the first genetic suppressors that eradicate FUS aggregates.

Hsp104^{A503X} variants suppress α-syn toxicity and promote its proper localization

Next, we tested Hsp104^{A503X} variants against α-syn toxicity in yeast. α-Syn is a lipid-binding protein that localizes to the plasma membrane, but forms cytoplasmic inclusions in degenerating dopaminergic neurons in PD and in yeast (Cushman et al., 2010; Outeiro and Lindquist, 2003). Nearly all Hsp104^{A503X} variants suppressed α-syn toxicity except Hsp104^{A503P}, which had no effect (Fig. 4A, B, S3C). By contrast, Hsp104^{WT} slightly enhanced α-syn toxicity (Figure 4A, B). Hsp104$^{A503V\text{-}DPLF}$ suppressed α-syn toxicity, though not as strongly as Hsp104^{A503V} (Fig. 4A). Rescue of α-syn toxicity by Hsp104^{A503X} variants (or Hsp104^{D504V}) could not be explained by: lower α-syn levels, induction of Hsp70 or Hsp26 in a HSR, or higher Hsp104 levels (Fig. 4C). Quantitative immunoblot indicated that the Hsp104 hexamer:α-syn ratios were ~1:2.43 for Hsp104^{WT} and ~1:2.84 for Hsp104^{A503V}. Expression of Hsp104^{A503V} from the Hsp104 promoter suppressed α-syn toxicity, whereas Hsp104^{WT} had no effect (Fig. S4E, F). Here, quantitative immunoblot indicated that the Hsp104 hexamer:α-syn ratios were ~1:3.03 for Hsp104^{WT} and ~1:5.79 for Hsp104^{A503V}. Hsp104^{A503V}, Hsp104^{A503S}, and Hsp104$^{A503V\text{-}DPLF}$ rescued α-syn toxicity in Δ*ire1* and Δ*atg8* strains (Fig. 4D). Thus, the UPR and autophagy are not required for rescue.

Hsp104^{A503V} eliminated cytoplasmic α-syn inclusions and restored plasma membrane α-syn localization, whereas Hsp104^{WT} had no effect (Fig. 4E). Indeed, Hsp104^{A503V} reduced the amount of insoluble α-syn by ~66%, whereas Hsp104^{WT} increased it by ~33.9% (Fig. 4F). Thus, potentiated Hsp104 variants eradicate α-syn inclusions and restore α-syn localization.

Potentiated Hsp104 variants prevent neurodegeneration in a *C. elegans* PD model

To test potentiated Hsp104 variants in a metazoan nervous system, we used a transgenic *C. elegans* PD model, which has illuminated mechanisms and modifiers of α-syn-induced neurodegeneration (Cao et al., 2005; Cooper et al., 2006; Tardiff et al., 2013). We selected Hsp104^{A503S} and Hsp104$^{A503V\text{-}DPLF}$ to study in this context, which displayed strong (Hsp104^{A503S}) and moderate (Hsp104$^{A503V\text{-}DPLF}$) rescue of α-syn toxicity (Fig. 4A). We focused on these variants because unlike Hsp104^{A503V} they conferred greater than WT levels of thermotolerance and were less toxic to yeast at 37°C when expressed from the galactose promoter (Fig. S5A, B).

The dopamine transporter (*dat-1*) gene promoter was used to direct expression of Hsp104 variants and α-syn to dopaminergic (DA) neurons. Expression of α-syn alone resulted in ~16% of animals with normal numbers of DA neurons after 7 days and ~8% of animals after 10 days compared to controls (Fig. 5A–C). Coexpression of Hsp104^{WT} or an ATPase-dead, substrate binding-deficient Hsp104$^{DPLA\text{-}DWB}$ (which bears the “double pore loop” and “double Walker B” mutations: Y257A:E285Q:Y662A:E687Q) did not rescue neurodegeneration (Fig. 5A, B). *C. elegans* expressing Hsp104^{A503S} and Hsp104$^{A503V\text{-}DPLF}$ displayed significant protection (30.5% and 34% normal worms, respectively) compared to the null Hsp104 variant or α-syn alone at day 7 (Fig. 5A). This trend continued at day 10 (Fig. 5B), when Hsp104^{A503S} (21%) and Hsp104$^{A503V\text{-}DPLF}$ (24%) expressing worms had significantly more normal DA neurons compared to α-syn alone (7.8%), Hsp104$^{DPLA\text{-}DWB}$ (10%), or Hsp104^{WT} (11%). Hsp104 variants did not alter α-syn mRNA levels (Fig. S5C). Thus, Hsp104^{A503S} and Hsp104$^{A503V\text{-}DPLF}$ remain significantly neuroprotective against α-syn toxicity even as animals age.

Potentiated Hsp104 variants typically have elevated ATPase activity

Nearly all of the Hsp104^{A503X} variants suppressed α-syn, FUS, and TDP-43 toxicity in yeast. This unexpected degeneracy is intriguing as there are few, if any, examples of missense mutations to nearly *any* class of residue that lead to a therapeutic gain of function.

To explore the mechanism behind this gain of function, we assessed the biochemical properties of several Hsp104 variants that suppressed toxicity. Each of $Hsp104^{A503X}$ variant and $Hsp104^{Y507C}$ exhibited ~2-4-fold higher ATPase activity than $Hsp104^{WT}$ (Fig. 6A). $Hsp104^{D498V}$ has higher ATPase activity than $Hsp104^{WT}$, though not as high as the $Hsp104^{A503X}$ variants (Fig. 6A). $Hsp104^{D504C}$ had similar ATPase activity to $Hsp104^{WT}$ (Fig. 6A). Thus, enhanced Hsp104 variants typically have higher ATPase activity than $Hsp104^{WT}$. However, $Hsp104^{D504C}$ illustrates that elevated ATPase activity is not absolutely required for potentiation.

Potentiated Hsp104 variants do not require Hsp70 and Hsp40 for disaggregation

Rescue of toxicity by enhanced Hsp104 variants might reflect an altered mechanism of disaggregation. Thus, we assessed activity against disordered luciferase aggregates (DeSantis et al., 2012). $Hsp104^{WT}$ was inactive alone and required Hsp70 and Hsp40, which could be from human (Hsc70 and Hdj2) or yeast (Ssa1 and Ydj1; Fig. 6B, C). By contrast, potentiated Hsp104 variants were extremely active without Hsp70 and Hsp40, and with the exception of $Hsp104^{D504C}$, Hsc70 and Hdj2 further increased activity (Fig. 6B, C). Typically, in the absence of Hsc70 and Hdj2, potentiated Hsp104 variants were ~3-9-fold more active than $Hsp104^{WT}$ plus Hsc70 and Hdj2 (Fig. 6B). The only exception was $Hsp104^{D498V}$, which in the absence of Hsc70 and Hdj2 was still as active as $Hsp104^{WT}$ plus Hsc70 and Hdj2 (Fig. 6B). $Hsp104^{WT}$ was most active in the presence of Ssa1, Ydj1, and the Hsp110, Sse1 (Fig. 6C) (Shorter, 2011). However, even here, $Hsp104^{WT}$ luciferase reactivation activity only reached $Hsp104^{A503V}$, $Hsp104^{A503S}$, and $Hsp104^{A503V\text{-}DPLF}$ activity in the absence of Ssa1, Ydj1, and Sse1 (Fig. 6C). In the presence of Ssa1, Ydj1, and Sse1, the luciferase reactivation activity of $Hsp104^{A503V}$, $Hsp104^{A503S}$, and $Hsp104^{A503V\text{-}DPLF}$ was ~7-8-fold higher than $Hsp104^{WT}$ (Fig. 6C). Potentiated Hsp104 variants are highly active without Hsp70 and Hsp40 (Fig. 6B, C). Thus, absolute dependence on Hsp70 and Hsp40 hinders Hsp104 from rescuing α-syn, FUS, and TDP-43 toxicity. Independence from Hsp70 and Hsp40 is promising for applying Hsp104 variants to reverse protein misfolding in diverse systems, such as purification of aggregation-prone recombinant proteins from *E. coli* where DnaK incompatibility is an issue (DeSantis and Shorter, 2012).

Potentiated Hsp104 variants translocate substrate faster than $Hsp104^{WT}$

We next determined that potentiated Hsp104 variants displayed accelerated substrate translocation. Thus, we used an Hsp104 variant, termed HAP, where G739-K741 is mutated to IGF, which enables association with the chambered peptidase ClpP (Tessarz et al., 2008). In the presence of ClpP, translocated substrates are degraded rather than released. Thus, HAP translocates FITC-casein for degradation by ClpP thereby releasing FITC and increasing fluorescence. In the presence of ClpP, HAP^{A503V} (K_m~1.29μM) is a more effective FITC-casein translocase than HAP^{WT} (K_m ~2.88μM) (Fig. 6D). The lower K_m for HAP_{A503V} might reflect differences in substrate recognition rather than translocation speed. However, the K_d of $Hsp104^{WT}$ (K_d~65nM) and $Hsp104^{A503V}$ (K_d ~80nM) for FITC-casein were similar (Fig. 6E) as were binding kinetics (Fig. 6F). Thus, substrate recognition by $Hsp104^{WT}$ and $Hsp104_{A503V}$ is very similar. Hence, we suggest that $Hsp104^{A503V}$ translocates substrate more rapidly than $Hsp104^{WT}$. Accelerated translocation likely enables potentiated variants to avoid kinetic traps and exert additional force to unfold stable substrates.

Potentiated Hsp104 variants are enhanced unfoldases

Next, we established that enhanced Hsp104 variants had enhanced unfoldase activity using a $RepA_{1–70}$-GFP substrate (Doyle et al., 2007). To assess $RepA_{1–70}$-GFP unfolding in the

absence of spontaneous refolding we added GroEL^{trap}, which captures unfolded proteins and prevents refolding (Weber-Ban et al., 1999). Hsp104^{WT} unfolds RepA$_{1–70}$-GFP but only in the presence of a permissive ratio of ATP and ATPγS (Doyle et al., 2007) (Fig. 6G, H). Thus, with ATP alone, Hsp104^{WT} did not unfold RepA$_{1–70}$-GFP (Fig. 6G). By contrast, Hsp104^{A503X} variants rapidly unfolded RepA$_{1–70}$-GFP in the presence of ATP (Fig. 6G). Hsp104^{WT} unfolded RepA$_{1–70}$-GFP in the presence of an ATP:ATPγS (3:1) mixture. By contrast, ATP:ATPγS slightly inhibited Hsp104^{A503V} unfoldase activity, but even here, Hsp104^{A503V} unfolded RepA$_{1–70}$-GFP more rapidly than Hsp104^{WT} (Fig. 6G). Hsp104^{A503X} variants had very similar unfoldase kinetics (Fig. 6G). By contrast, Hsp104^{D498V}, Hsp104^{D504C}, and Hsp104$^{A503V\text{-}DPLF}$ were slightly slower unfoldases than Hsp104^{A503V}, whereas Hsp104^{Y507C} was slightly faster (Fig. 6H). These differences could reflect changes in substrate recognition or turnover or both. Regardless, potentiated Hsp104 variants are enhanced unfoldases that are intrinsically primed to unfold substrates and do not have to wait for regulatory events (mimicked here by ATPγS addition).

Hsp104^{A503V} hexamers are tuned differently than Hsp104^{WT} hexamers

Do potentiated Hsp104 variants employ the same mechanism of intersubunit collaboration as Hsp104^{WT} to disaggregate proteins? How Hsp104 subunits within the hexamer collaborate to promote disaggregation can be interrogated via mutant subunit doping. Here, mutant subunits defective in ATP hydrolysis, substrate binding, or both, are mixed with WT subunits to generate heterohexamer ensembles according to the binomial distribution (DeSantis et al., 2012). Hsp104 forms dynamic hexamers that exchange subunits on the minute timescale, which ensures statistical incorporation of mutant subunits (DeSantis et al., 2012). The disaggregase activity of various heterohexamer ensembles enables determination of the number of mutant subunits that inactivate the WT hexamer. Thus, we can determine if subunit collaboration within Hsp104 hexamers is probabilistic (six mutant subunits are required to abolish activity), subglobally cooperative (two to five mutant subunits abolish activity), or globally cooperative (one mutant subunit abolishes activity) (DeSantis et al., 2012). Incorporation of Hsp104$^{A503V\text{-}DWA}$ subunits (which bear the “double Walker A” [DWA] K218T:K620T mutations and cannot bind ATP) or Hsp104$^{A503V\text{-}DPLA}$ subunits (which bear the “double pore loop” [DPL] Y257A:Y662A mutations and cannot bind substrate) into Hsp104^{A503V} hexamers caused a roughly linear decline in luciferase disaggregase activity (Fig. 6I). This linear decline indicates that like Hsp104^{WT}, Hsp104^{A503V} hexamers resolve disordered aggregates via a probabilistic mechanism (DeSantis et al., 2012). Thus, a single Hsp104^{A503V} subunit per hexamer able to hydrolyze ATP and engage substrate can drive disaggregation.

However, Hsp104^{A503V} hexamers operate differently than Hsp104^{WT} hexamers. A single Hsp104^{DWB} subunit (which bear the “double Walker B” [DWB] E285Q:E687Q mutations and can bind but not hydrolyze ATP) inactivates the Hsp104^{WT} hexamer (DeSantis et al., 2012). By contrast, the luciferase disaggregase activity of Hsp104^{A503V} was stimulated by Hsp104$^{A503V\text{-}DWB}$ subunits (Fig. 6J). FRET studies confirmed that Hsp104$^{A503V\text{-}DWB}$ subunits incorporated into Hsp104^{A503V} hexamers. The FRET efficiency was 0.36 (compared to 0.38 for mixing Hsp104^{WT} with Hsp104^{DWB} (DeSantis et al., 2012)) using the conditions employed for luciferase reactivation. In high salt buffer (1M NaCl), hexamerization is inhibited and FRET efficiency decreased to 0.24. At higher Hsp104 concentration (1μM), which favors hexamerization, FRET efficiency increased to 0.43. We could model the stimulatory effect of Hsp104$^{A503V\text{-}DWB}$ subunits if we imposed rules whereby an Hsp104$^{A503V\text{-}DWB}$ subunit stimulates activity of an adjacent Hsp104^{A503V} subunit ~2-fold (Fig. 6J). This stimulation depended on substrate-binding by Hsp104$^{A503V\text{-}DWB}$ as Hsp104$^{A503V\text{-}DPLA\text{-}DWB}$ subunits (which bear the “double pore loop” and “double Walker B” Y257A:E285Q:Y662A:E687Q mutations and can bind but not

hydrolyze ATP and cannot bind substrate) failed to stimulate adjacent Hsp104^{A503V} subunits (Fig. 6J). Thus, Hsp104^{A503V} hexamers operate via principles distinct from those of Hsp104^{WT} hexamers. The Hsp104^{A503V} hexamer displays greater plasticity and tolerates a wider variety of subunit-inactivating events to maintain a robust disaggregase activity. Thus, an Hsp104^{A503V} subunit that: (1) binds but cannot hydrolyze ATP and (2) engages substrate, stimulates the disaggregase activity of an adjacent Hsp104^{A503V} subunit. In Hsp104^{WT}, a single subunit with these properties inactivates the hexamer. The increased resilience of Hsp104^{A503V} hexamers to subunit-inactivating events likely empowers facile resolution of recalcitrant substrates.

Hsp104^{A503V}, Hsp104^{A503S}, and Hsp104$^{A503V\text{-}DPLF}$ disaggregate *preformed* α-syn fibrils more efficaciously than Hsp104^{WT}

To test Hsp104^{A503V}, Hsp104^{A503S}, and Hsp104$^{A503V\text{-}DPLF}$ in comparison to Hsp104^{WT} against a recalcitrant PD-associated substrate we employed α-syn fibrils, allowing us to distinguish if Hsp104 prevented amyloid formation or eliminated preformed amyloid. Hsp104^{A503V}, Hsp104^{A503S}, and Hsp104$^{A503V\text{-}DPLF}$ disaggregated preformed α-syn fibrils at concentrations where Hsp104^{WT} was inactive (Fig. 7A–C). Indeed, electron microscopy (EM) revealed that α-syn fibrils were converted to small structures by low concentrations of Hsp104^{A503V}, Hsp104^{A503S}, and Hsp104$^{A503V\text{-}DPLF}$, whereas Hsp104^{WT} left fibrils intact (Fig. 7C). Thus, Hsp104^{A503V}, Hsp104^{A503S}, and Hsp104$^{A503V\text{-}DPLF}$ are more powerful amyloid disaggregases than Hsp104^{WT}.

Hsp104^{A503V} and Hsp104^{A503S} disaggregate *preformed* TDP-43 and FUS aggregates more efficaciously than Hsp104^{WT}

Next, we tested whether Hsp104^{A503V} and Hsp104^{A503S} were more potent disaggregases of TDP-43 and FUS (Johnson et al., 2009; Sun et al., 2011). Hsp104^{WT} was unable to resolve TDP-43 aggregates and slightly enhanced TDP-43 aggregation in the absence of Ssa1, Ydj1, and Sse1 (Fig. 7D). By contrast, Hsp104^{A503V} and Hsp104^{A503S} partially resolved TDP-43 aggregates in the absence of Ssa1, Ydj1, and Sse1 (Fig. 7D). Hsp104^{A503V} and Hsp104^{A503S} in the presence of Ssa1, Ydj1, and Sse1, but not by Hsp104^{WT}, effectively dissolved short TDP-43 filaments and amorphous structures (Fig. 7D, E). Very similar results were obtained with preformed FUS fibrils (Fig. 7F, G). Hsp104^{WT} slightly increased FUS aggregation in the absence of Ssa1, Ydj1, and Sse1, whereas Hsp104^{A503V} and Hsp104^{A503S} modestly reduced aggregation (Fig. 7F). Hsp104^{A503V} and Hsp104^{A503S} effectively disaggregated FUS in the presence of Ssa1, Ydj1, and Sse1, whereas Hsp104^{WT} was ineffective (Fig. 7F). Indeed, Hsp104^{A503V} and Hsp104^{A503S} eradicated FUS fibrils (Fig. 7G). Thus, Hsp104^{A503V} and Hsp104^{A503S} disaggregate preformed TDP-43 and FUS aggregates more efficaciously than Hsp104^{WT}.

Discussion

Here, we demonstrate that Hsp104, a protein disaggregase from yeast, can be modified to powerfully eradicate diverse substrates implicated in ALS and PD. We have developed the first, to our knowledge, disaggregases (or even chaperones) engineered to optimize proteostasis. Indeed, enhanced Hsp104 variants are the first agents defined to reverse TDP-43 and FUS aggregation. They not only suppress toxicity and eliminate protein aggregates, but also restore proper protein localization. Importantly, these Hsp104 variants are not overtly toxic like other MD mutants (Lipinska et al., 2013). Thus, potentiated Hsp104 variants can be uncovered that are not invariably toxic and which rescue various toxic neurodegenerative disease proteins in vitro and in vivo under conditions where Hsp104^{WT} is impotent. Potentiated Hsp104 variants suppress neurodegeneration in a *C. elegans* PD model. Thus, we provide the first example of engineered disaggregases rescuing

neurodegeneration in a metazoan nervous system under conditions where the WT disaggregase is ineffective. Our findings suggest that general neuroprotection via activated protein disaggregases may be possible for diverse neurodegenerative diseases.

We have identified the MD as a key region governing Hsp104 function. It is perplexing and unprecedented that missense mutations to nearly any residue at specific and disparate positions (e.g. A503, Y507) confers a therapeutic gain of function. Potentiation stems from loss of amino acid identity rather than specific mutation. Thus, Hsp104 activity is likely tightly constrained but can be unleashed by subtle changes to side chains at specific positions. These constraints are too tight for $Hsp104^{WT}$ to counter TDP-43, FUS, and α-syn aggregation and toxicity under the conditions employed in our experiments. Thus, we reveal a surprising inimical deficit in existing disaggregase functionality. We suggest that the MD functions as a capacitor braced to unleash Hsp104 activity. Missense mutations at specific positions in MD helix 1, 2, or 3 or the small domain of NBD1 (immediately C-terminal to the MD) likely destabilize autoinhibitory interactions that dampen Hsp104 activity or induce conformational changes that mimic or aid in an allosteric activation step. Potentiating mutations obviate any absolute requirement for Hsp70 and enhance Hsp104 ATPase activity, substrate translocation speed, unfoldase activity, and amyloid disaggregase activity. Additionally, $Hsp104^{A503V}$ hexamers display enhanced plasticity and are more resistant to defective subunits than $Hsp104^{WT}$. Thus, enhanced variants possess a more robust disaggregase activity that is desensitized to inhibition. Irrespective of the mechanism of activation, we have established that seemingly minor structural modulation of a disaggregase can suppress a constellation of otherwise intractable proteotoxicities in vivo. We are unaware of any precedent for attaining such a wide-reaching set of gain of therapeutic functions via such minor changes in primary sequence, e.g. by removing a single methyl group (A503G) or by adding a single methylene bridge (V426L).

Further engineering to develop enhanced variants that specifically target single proteins (e.g. disaggregate FUS but not TDP-43) will prove valuable to minimize any off-target effects. Hsp104 could be potentiated against any protein, which might find key applications in purification of troublesome recombinant proteins. Irrespective of the feasibility of introducing Hsp104 as a therapeutic, our work suggests that protein aggregates are not intractable and that general neuroprotection via altered proteostasis is achievable. Ultimately, we envision introducing potentiated Hsp104 variants in short transient bursts to restore natural proteostasis. In this way, long-term expression of an exogenous protein is avoided. Reactivation of disease-associated proteins to their non-pathogenic states suggests that Hsp104 variants and other agents that achieve this goal may be highly promising for halting and reversing neurodegenerative disease. Nonetheless, caution is needed and many barriers must be breached to translate Hsp104 variants into disruptive technologies and potential therapeutics.

Experimental Procedures

Yeast strains and media

Yeast were WT W303a or the isogenic W303aΔ*hsp104* strain. Δ*ire1* and Δ*atg8* were in BY4741. Standard methods were used for transformation and spotting. See Extended Experimental Procedures.

Library Construction and Screening

The pore loop variant library was constructed via QuikChange mutagenesis (Agilent) and DNA shuffling to obtain randomly combined residues at positions Y257 and Y662. The MD variant library was constructed using GeneMorph II EZClone Domain Mutagenesis kit

(Agilent) with modifications. Libraries were transformed into yeast harboring pAG303GAL-TDP-43, pAG303GAL-FUS, or pAG303GAL-α-syn. Yeast were grown overnight in raffinose-containing media and plated on galactose-containing media for selection. Select colonies were sequenced by colony PCR. Isolated Hsp104 variants were cloned independently and transformed into yeast to ensure they suppressed toxicity. See Extended Experimental Procedures.

Hsp104 Variant Toxicity and Thermotolerance

W303Δ*hsp104* yeast were transformed with the indicated 416GAL-Hsp104 plasmid. Cultures were grown in synthetic raffinose medium to A_{600nm}=2.0, spotted onto SD-Ura or SGal-Ura, and incubated at 30°C or 37°C for 48–72h. For thermotol erance, yeast were grown to saturation in synthetic raffinose media and diluted to A_{600nm}=0.3 in galactose-containing media. After 4h at 30°C, cells were heat shocked at 50°C for 0–30min, cooled for 2min on ice, serially diluted, and spotted on synthetic dropout media containing galactose. Plates were incubated at 30°C for 48–72h.

Sedimentation Analysis

Yeast were induced in galactose-containing medium for 5h (TDP-43 and FUS) or 8h (α-syn). Cells were lysed, separated into soluble and insoluble fractions by sedimentation, and processed for quantitative immunoblot. See Extended Experimental Procedures.

Fluorescence Microscopy

After 5h induction at 30°C (8h for α-syn strains), yeast cultures were processed for fluorescence microscopy. For TDP-43, cells were fixed and stained with 4',6-diamidino-2-phenylindole (DAPI) to visualize nuclei. For FUS, live cells were used and nuclei were visualized with Hoechst dye. See Extended Experimental Procedures.

Analysis for Dopaminergic Neuron Death in *C. elegans*

Three distinct *C. elegans* stable lines were created for each Hsp104 variant. Age synchronized worms were generated by allowing 50 transgenic adults on a NGM plate to lay eggs for 3h. Adults were then removed (day 0). At day 7 and 10 of analysis, 40 randomly selected transgenic worms were placed in 3mM Levamisol for paralysis and transferred to a 2% agarose pad on a glass microscope slide. Worms have 8 dopaminergic neurons visible through Pdat-1::gfp, which fade in an age-dependent manner due to α-syn accumulation. Only the 6 anterior neurons of the worm were analyzed. Each worm was scored "Wild type" when there was a full complement of visible, anterior dendritic processes. Worms missing one or more dendritic processes was scored "Not Wild Type". In total three separate stable lines were analyzed. See Extended Experimental Procedures.

Protein Purification

Proteins were purified as recombinant proteins in *E. coli* using standard techniques. See Extended Experimental Procedures.

ATPase activity

Hsp104 (0.042μM hexamer) was incubated with ATP (1mM) for 5min at 25°C. ATPase activity was assessed by inorganic phosphate release using a malachite green detection kit (Innova).

Luciferase Reactivation

Aggregated luciferase (50nM) was incubated with Hsp104 (0.167 μM hexamer) with ATP (5.1mM) and an ATP regeneration system (ARS; 1mM creatine phosphate, 0.25μM creatine kinase) plus or minus Hsc70 (0.167μM) and Hdj2 (0.167μM) for 90min at 25°C (DeSantis et al., 2012). In some reactions (Fig. 6C), Hsc70 concentration was 0.167μM and Hdj2 concentration was 0.073μM. In other reactions, Hsc70 and Hdj2 were replaced with Ssa1 (0.167μM) and Ydj1 (0.073μM) or Ssa1 (0.167μM), Ydj1 (0.073μM), and Sse1 (0.043μM). Luciferase activity was assessed by luminescence. Mutant doping experiments were as described (DeSantis et al., 2012). $Hsp104^{A503V}$ variants: $Hsp104^{A503V\text{-}DWA}$ (K218T:A503V:K620T), $Hsp104^{A503V\text{-}DPLA}$ (Y257A:A503V:Y662A), $Hsp104^{A503V\text{-}DWB}$ (E285Q:A503V:E687Q), $Hsp104^{A503V\text{-}DPLA\text{-}DWB}$ (Y257A:E285Q:A503V:Y662A:E687Q) were mixed with $Hsp104^{A503V}$ in varying ratios to give a total concentration of 0.5μM Hsp104 hexamer. Hsc70 and Hdj2 were omitted for these experiments. Random subunit mixing was confirmed by FRET. See Extended Experimental Procedures.

$RepA_{1-70}$-GFP Unfolding

$RepA_{1-70}$-GFP unfolding was as described (Doyle et al., 2007).

FITC-Casein Degradation and Binding

FITC-casein (0.1–50μM) was incubated at 25°C with HAP or HAP^{A503V} (1μM hexamer) and ClpP (21μM monomer) plus ATP (5mM) and ARS. Degradation of FITC-casein was monitored by fluorescence (excitation 490nm, emission 520nm). To calculate initial rate, a linear fit of the first 2.5min of the reaction was constructed and the slope was calculated. To assess binding, FITC-casein (6nM) was incubated with increasing concentrations (0–5μM) of $Hsp104^{WT}$ or $Hsp104^{A503V}$ with 2mM ATPγS for 10min at 25°C. Fluorescence polarization was measured (excitation 470nm, emission 520nm).

α-syn fibril disaggregation

α-syn (80μM) was assembled into fibrils via incubation in 40mM HEPES-KOH, pH 7.4, 150mM KCl, 20mM $MgCl_2$, 1mM DTT for 48h at 37°C with agitation. α-syn fibrils (0.5μM monomer) were incubated without or with $Hsp104^{WT}$, $Hsp104^{A503V}$, $Hsp104^{A503S}$, or$Hsp104^{A503V\text{-}DPLF}$ (0.5 or 5μM) plus ATP (10mM) and ARS (20mM creatine phosphate and 0.5μM creatine kinase) for 1h at 30°C. Disaggregation was assessed by Thioflavin-T (ThT) fluorescence, sedimentation analysis, and EM (Lo Bianco et al., 2008).

TDP-43 and FUS disaggregation

To generate TDP-43 and FUS aggregates, GST-TEV-TDP-43 (6μM) or GST-TEV-FUS (6μM) were incubated with TEV protease in 50mM TrisHCl pH 7.4, 50mM KCl, 5mM $MgCl_2$, 0.2M trehalose, and 20mM glutathione. FUS was aggregated for 90min at 25°C without agitation, by which time all the FUS had aggregated (Sun et al., 2011). TDP-43 was aggregated for 4h at 25°C with agitation, by which time all the TDP-43 h ad aggregated (Johnson et al., 2009). TDP-43 or FUS aggregates (3μM monomer) were incubated for 1h at 30°C with $Hsp104^{WT}$, $Hsp104_{A503V}$, or $Hsp104^{A503S}$ (1μM) plus or minus Ssa1 (1μM), Ydj1 (0.44μM), and Sse1 (0.26μM) plus ATP (10mM) and ARS (20mM creatine phosphate and 0.5μM creatine kinase). Disaggregation was assessed via turbidity (absorbance at 395nm) and EM (Johnson et al., 2009; Sun et al., 2011).

Supplementary Material

Refer to Web version on PubMed Central for supplementary material.

Acknowledgments

We thank Sue Lindquist, Johannes Buchner, Walid Houry, Aaron Gitler, Martin Duennwald, and Brad Johnson for kindly sharing reagents; Beatrice Razzo and Nabeel Akhtar for help in library construction and screening; Mark Lemmon, Mariana Torrente, and Liz Sweeny for critiques. Our studies were supported by: an American Heart Association Post-Doctoral Fellowship (M.E.J); NIH training grant (T32GM071339) and NRSA predoctoral fellowship F31NS079009 (M.E.D.); NSF Graduate Research Fellowship DGE-0822 (L.M.C.); NSF CAREER Award 0845020 (K.A.C.); NIH grant R15NS075684 (G.A.C); NIH Director's New Innovator Award DP2OD002177, NIH grants R21NS067354, R21HD074510, and R01GM099836, a Muscular Dystrophy Association Research Award (MDA277268), Packard Center for ALS Research at Johns Hopkins University, Target ALS, and an Ellison Medical Foundation New Scholar in Aging Award (J.S.).

Literature Cited

Cao S, Gelwix CC, Caldwell KA, Caldwell GA. Torsin-mediated protection from cellular stress in the dopaminergic neurons of *Caenorhabditis elegans*. J Neurosci. 2005; 25:3801–3812. [PubMed: 15829632]

Cooper AA, Gitler AD, Cashikar A, Haynes CM, Hill KJ, Bhullar B, Liu K, Xu K, Strathearn KE, Liu F, et al. Alpha-synuclein blocks ER-Golgi traffic and Rab1 rescues neuron loss in Parkinson's models. Science. 2006; 313:324–328. [PubMed: 16794039]

Cushman M, Johnson BS, King OD, Gitler AD, Shorter J. Prion-like disorders: blurring the divide between transmissibility and infectivity. J Cell Sci. 2010; 123:1191–1201. [PubMed: 20356930]

Cushman-Nick M, Bonini NM, Shorter J. Hsp104 Suppresses Polyglutamine-Induced Degeneration Post Onset in a Drosophila MJD/SCA3 Model. PLoS genetics. 2013; 9:e1003781. [PubMed: 24039611]

DeSantis ME, Leung EH, Sweeny EA, Jackrel ME, Cushman-Nick M, Neuhaus-Follini A, Vashist S, Sochor MA, Knight MN, Shorter J. Operational plasticity enables hsp104 to disaggregate diverse amyloid and nonamyloid clients. Cell. 2012; 151:778–793. [PubMed: 23141537]

DeSantis ME, Shorter J. The elusive middle domain of Hsp104 and ClpB: location and function. Biochim Biophys Acta. 2012; 1823:29–39. [PubMed: 21843558]

Doyle SM, Shorter J, Zolkiewski M, Hoskins JR, Lindquist S, Wickner S. Asymmetric deceleration of ClpB or Hsp104 ATPase activity unleashes protein-remodeling activity. Nat Struct Mol Biol. 2007; 14:114–122. [PubMed: 17259993]

Duennwald ML, Echeverria A, Shorter J. Small heat shock proteins potentiate amyloid dissolution by protein disaggregases from yeast and humans. PLoS Biol. 2012; 10:e1001346. [PubMed: 22723742]

Elden AC, Kim HJ, Hart MP, Chen-Plotkin AS, Johnson BS, Fang X, Armakola M, Geser F, Greene R, Lu MM, et al. Ataxin-2 intermediate-length polyglutamine expansions are associated with increased risk for ALS. Nature. 2010; 466:1069–1075. [PubMed: 20740007]

Johnson BS, McCaffery JM, Lindquist S, Gitler AD. A yeast TDP-43 proteinopathy model: Exploring the molecular determinants of TDP-43 aggregation and cellular toxicity. Proc Natl Acad Sci U S A. 2008; 105:6439–6444. [PubMed: 18434538]

Johnson BS, Snead D, Lee JJ, McCaffery JM, Shorter J, Gitler AD. TDP-43 is intrinsically aggregation-prone, and amyotrophic lateral sclerosis-linked mutations accelerate aggregation and increase toxicity. J Biol Chem. 2009; 284:20329–20339. [PubMed: 19465477]

Ju S, Tardiff DF, Han H, Divya K, Zhong Q, Maquat LE, Bosco DA, Hayward LJ, Brown RH Jr, Lindquist S, et al. A Yeast Model of FUS/TLS-Dependent Cytotoxicity. PLoS Biol. 2011; 9:e1001052. [PubMed: 21541368]

Lipinska N, Zietkiewicz S, Sobczak A, Jurczyk A, Potocki W, Morawiec E, Wawrzycka A, Gumowski K, Slusarz M, Rodziewicz-Motowidlo S, et al. Disruption of ionic interactions between the nucleotide binding domain 1 (NBD1) and middle (M) domain in Hsp100 disaggregase unleashes toxic hyperactivity and partial independence from Hsp70. J Biol Chem. 2013; 288:2857–2869. [PubMed: 23233670]

Lo Bianco C, Shorter J, Regulier E, Lashuel H, Iwatsubo T, Lindquist S, Aebischer P. Hsp104 antagonizes alpha-synuclein aggregation and reduces dopaminergic degeneration in a rat model of Parkinson disease. J Clin Invest. 2008; 118:3087–3097. [PubMed: 18704197]

Newby GA, Lindquist S. Blessings in disguise: biological benefits of prion-like mechanisms. Trends Cell Biol. 2013; 23:251–259. [PubMed: 23485338]

Outeiro TF, Lindquist S. Yeast Cells Provide Insight into Alpha-Synuclein Biology and Pathobiology. Science. 2003; 302:1772–1775. [PubMed: 14657500]

Robberecht W, Philips T. The changing scene of amyotrophic lateral sclerosis. Nat Rev Neurosci. 2013; 14:248–264. [PubMed: 23463272]

Saibil H. Chaperone machines for protein folding, unfolding and disaggregation. Nat Rev Mol Cell Biol. 2013; 13:630–642. [PubMed: 24026055]

Schirmer EC, Homann OR, Kowal AS, Lindquist S. Dominant gain-of-function mutations in Hsp104p reveal crucial roles for the middle region. Mol Biol Cell. 2004; 15:2061–2072. [PubMed: 14978213]

Shorter J. Hsp104: a weapon to combat diverse neurodegenerative disorders. Neurosignals. 2008; 16:63–74. [PubMed: 18097161]

Shorter J. The mammalian disaggregase machinery: Hsp110 synergizes with Hsp70 and Hsp40 to catalyze protein disaggregation and reactivation in a cell-free system. PloS one. 2011; 6:e26319. [PubMed: 22022600]

Sun Z, Diaz Z, Fang X, Hart MP, Chesi A, Shorter J, Gitler AD. Molecular Determinants and Genetic Modifiers of Aggregation and Toxicity for the ALS Disease Protein FUS/TLS. PLoS Biol. 2011; 9:e1000614. [PubMed: 21541367]

Tardiff DF, Jui NT, Khurana V, Tambe MA, Thompson ML, Chung CY, Kamadurai HB, Kim HT, Lancaster AK, Caldwell KA, et al. Yeast Reveal a "Druggable" Rsp5/Nedd4 Network that Ameliorates alpha-Synuclein Toxicity in Neurons. Science. 2013

Tessarz P, Mogk A, Bukau B. Substrate threading through the central pore of the Hsp104 chaperone as a common mechanism for protein disaggregation and prion propagation. Molecular Microbiology. 2008; 68:87–97. [PubMed: 18312264]

Vacher C, Garcia-Oroz L, Rubinsztein DC. Overexpression of yeast hsp104 reduces polyglutamine aggregation and prolongs survival of a transgenic mouse model of Huntington's disease. Human molecular genetics. 2005; 14:3425–3433. [PubMed: 16204350]

Weber-Ban EU, Reid BG, Miranker AD, Horwich AL. Global unfolding of a substrate protein by the Hsp100 chaperone ClpA. Nature. 1999; 401:90–93. [PubMed: 10485712]

- We reprogram Hsp104 to rescue TDP-43, FUS, and α-synuclein proteotoxicity
- Potentiated Hsp104 variants clear inclusions and restore proper protein localization
- Potentiating mutations reconfigure how Hsp104 hexamers operate
- Enhanced disaggregases can restore proteostasis and mitigate neurodegeneration

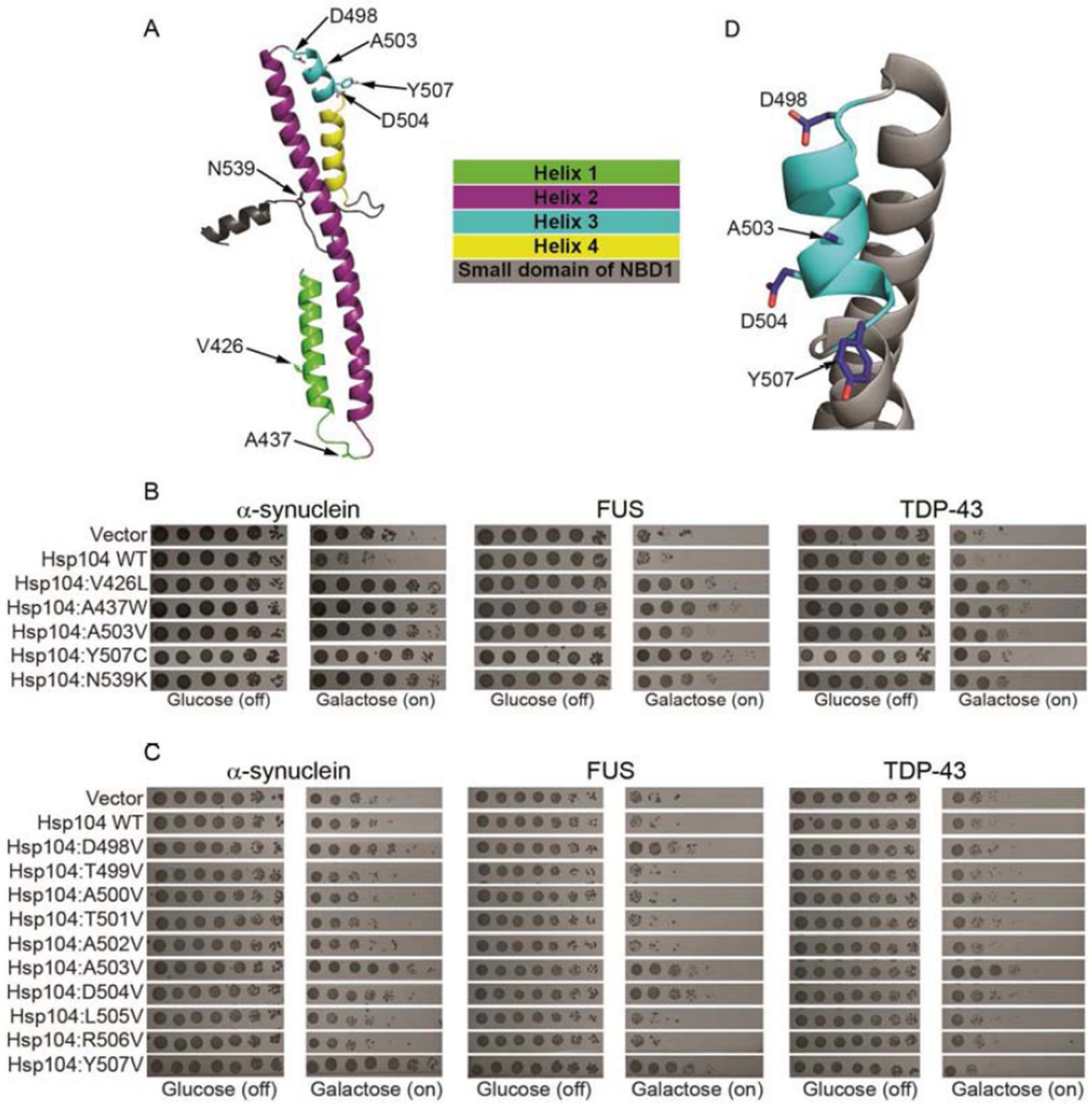

Figure 1. Hsp104 MD variants rescue diverse proteotoxicity models

(A) Homology model of the MD and a portion of the small domain of NBD1 of Hsp104. Side chains of key residues are shown as sticks. **(B)** Δ*hsp104* yeast strains integrated with galactose-inducible α-syn, FUS, or TDP-43 were transformed with the indicated Hsp104 variant or vector control. Strains were serially diluted fivefold and spotted on glucose (off) or galactose (on) media. **(C)** Hsp104 variants harboring missense mutations to valine ranging from residue D498 to Y507 were expressed with FUS, TDP-43, or α-syn. **(D)** Close-up of MD helix 3 from **(A)**. Mutation of D498, A503, D504, or Y507 activates Hsp104.

See also Fig. S1.

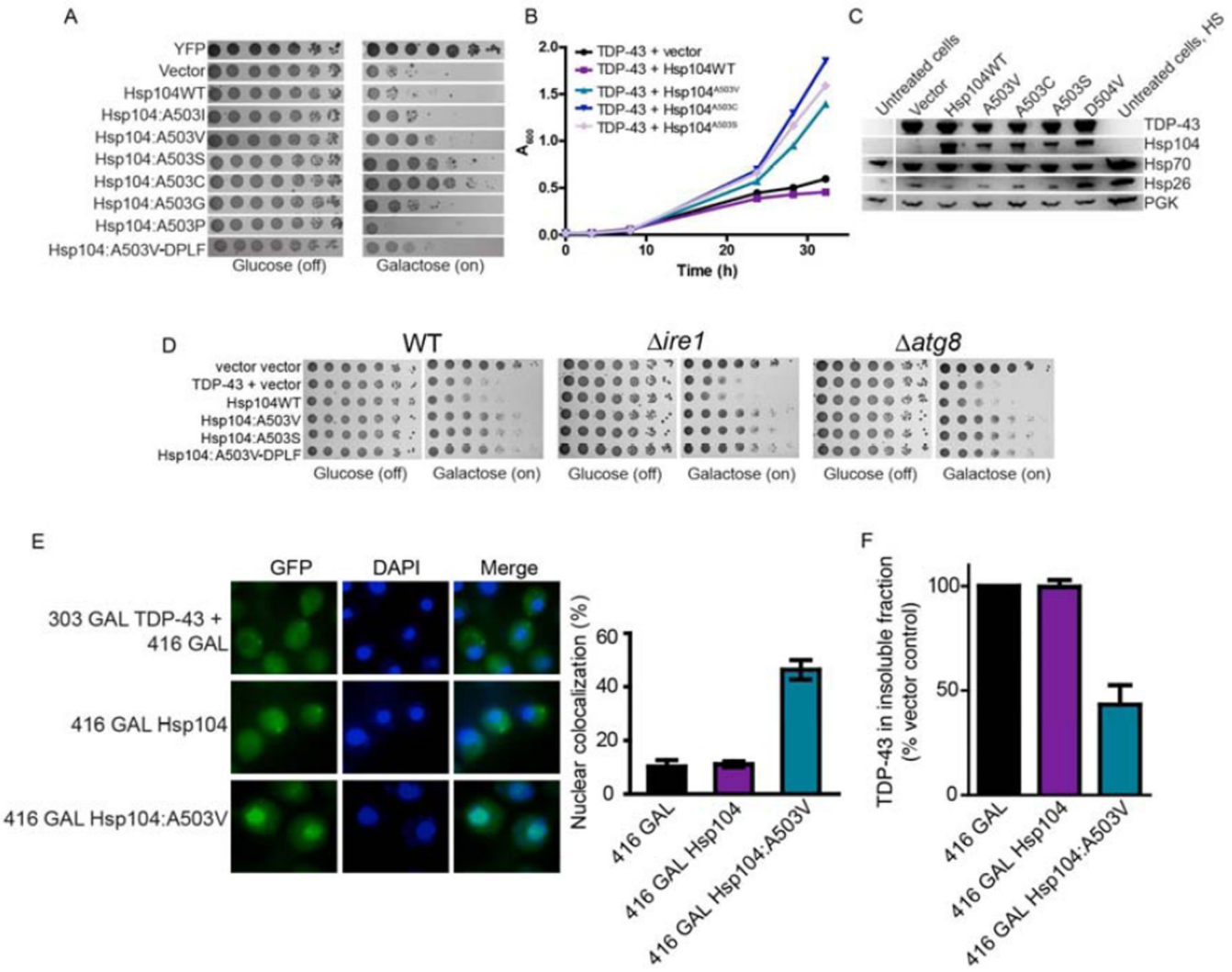

Figure 2. Hsp104$_{A503X}$ variants suppress TDP-43 toxicity, aggregation, and mislocalization

(A) Δ*hsp104* yeast transformed with TDP-43 and Hsp104 variants, or YFP and vector, were serially diluted fivefold and spotted onto glucose (off) or galactose (on). **(B)** Selected strains from **(A)** were induced in liquid and growth was monitored by A_{600nm}. **(C)** Strains from **(B)** were induced for 5h, lysed, and immunoblotted. Uninduced (untreated) and heat shocked cells (HS) serve as controls. 3-Phosphoglycerate kinase (PGK1) serves as a loading control. **(D)** WT, Δ*ire1*, or Δ*atg8* yeast were co-transformed with vector control, or TDP-43 plus vector, or the indicated Hsp104 variant and were serially diluted fivefold and spotted onto glucose (off) or galactose (on). **(E)** Fluorescence microscopy of cells co-expressing fluorescently tagged TDP-43 and Hsp104^{WT}, Hsp104^{A503V}, or vector. Cells were stained with DAPI to visualize nuclei (blue). TDP-43 localization was quantified by counting the number of cells containing colocalized nuclear staining. Values represent means±SEM (n=3). **(F)** Δ*hsp104* yeast co-transformed with TDP-43 and vector or the indicated Hsp104 variant were induced with galactose for 5h at 30°C, lysed and processed for s edimentation analysis and quantitative immunoblot. The relative amount of insoluble TDP-43 was determined as a % of the vector control. Values represent means±SEM (n=2).
See also Fig. S2, S3, and S4.

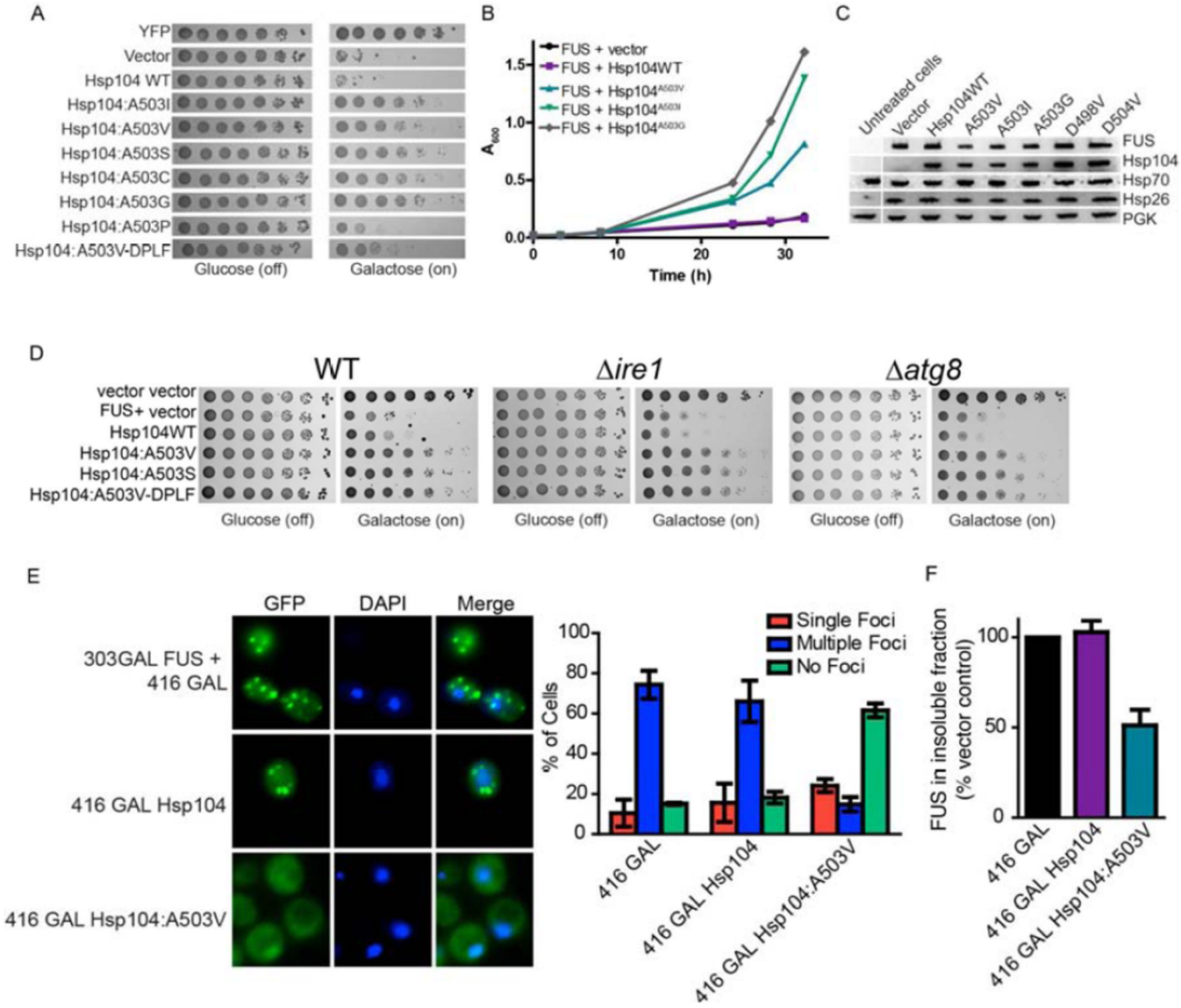

Figure 3. Hsp104^{A503X} variants suppress FUS toxicity and aggregation

(A) Δ*hsp104* yeast transformed with FUS and the Hsp104 variants, or YFP and vector, were serially diluted fivefold and spotted onto glucose (off) or galactose (on). **(B)** Selected strains from **(A)** were induced in liquid and growth was monitored by A_{600nm}. **(C)** Strains from **(B)** were induced for 5h, lysed, and immunoblotted. **(D)** WT, Δ*ire1*, or Δ*atg8* yeast were co-transformed with vector control, or FUS plus vector, or the indicated Hsp104 variant and were serially diluted fivefold and spotted onto glucose (off) or galactose (on). **(E)** Fluorescence microscopy of cells co-expressing FUS-GFP and Hsp104^{WT}, Hsp104^{A503V}, or vector. Cells were stained with Hoechst dye to visualize nuclei (blue). FUS aggregation was quantified by counting the number of cells containing 0, 1, or more than 1 foci. Values represent means±SEM (n=3). **(F)** Δ*hsp104* yeast co-transformed with FUS and vector or the indicated Hsp104 variant were induced with galactose for 5h at 30°C, lysed and processed for sedimentation analysis and quantitative immunoblot. The relative amount of insoluble FUS was determined as a % of the vector control. Values represent means±SEM (n=2). See also Fig. S3 and S4.

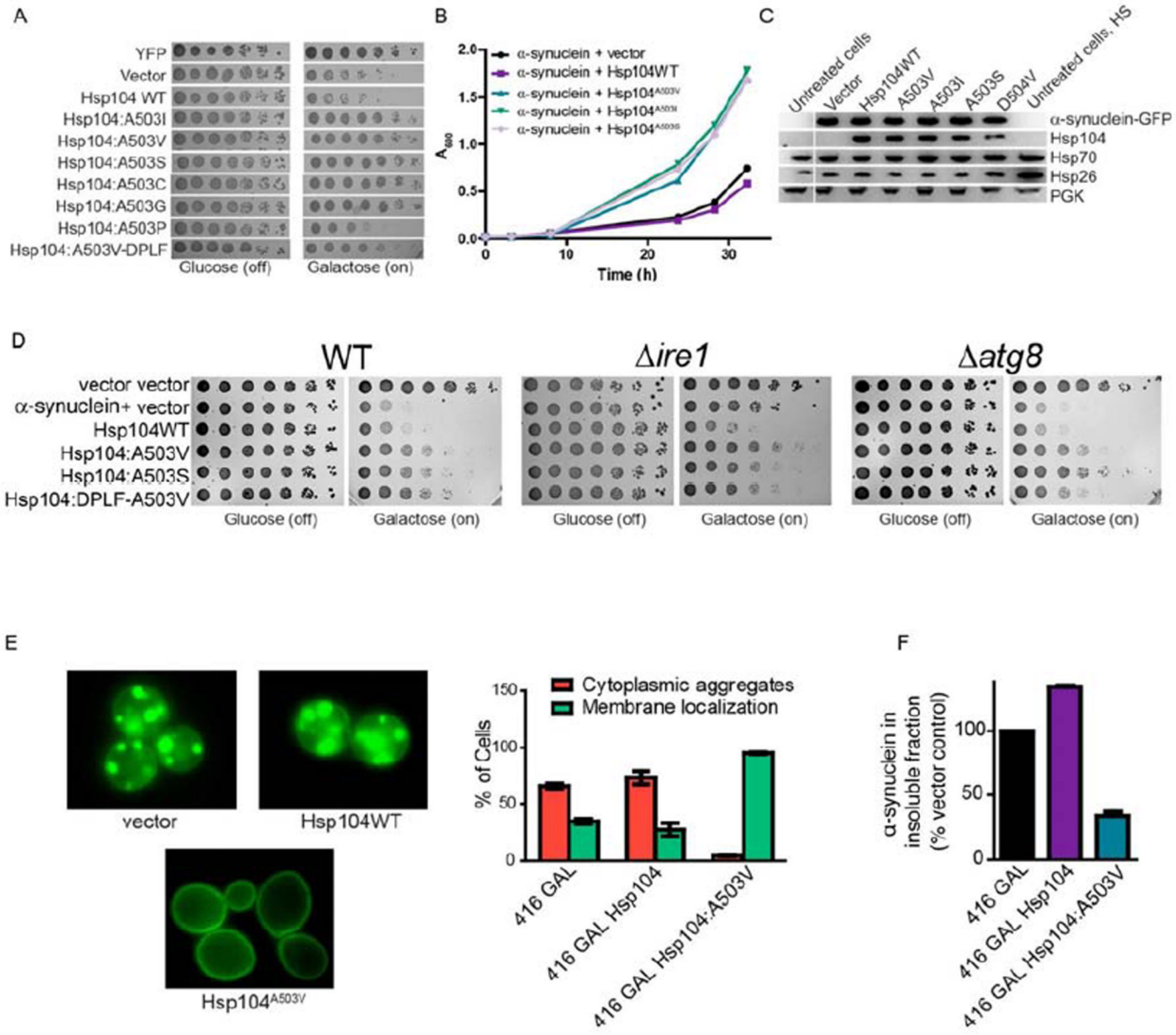

Figure 4. Hsp104^{A503X} variants suppress α-syn toxicity, aggregation, and mislocalization

(A) Δ*hsp104* yeast co-transformed with two copies of α-syn-YFP and the Hsp104 variants, or YFP and vector, were serially diluted fivefold and spotted onto glucose (off) or galactose (on). **(B)** Selected strains from **(A)** were induced in liquid and growth was monitored by A_{600nm}. **(C)** Strains from **(B)** were induced for 8h in galactose, lysed, and immunoblotted. **(D)** WT, Δ*ire1*, or Δ*atg8* yeast were co-transformed with vector controls, or α-syn plus vector or the indicated Hsp104 variant and were serially diluted fivefold and spotted onto glucose (off) or galactose (on). **(E)** Fluorescence microscopy of cells co-expressing α-syn-YFP and Hsp104^{WT}, Hsp104^{A503V}, or vector. α-Syn localization was quantified by counting the number of cells with plasma membrane fluorescence or cytoplasmic aggregates. Values represent means±SEM (n=3). **(F)** Δ*hsp104* yeast co-transformed with α-syn and vector or the indicated Hsp104 variant were induced with galactose for 8h at 30°C, lysed a nd processed for sedimentation analysis and quantitative immunoblot. The relative amount of insoluble α-syn was determined as a % of the vector control. Values represent means±SEM (n=2).

See also Fig. S3 and S4.

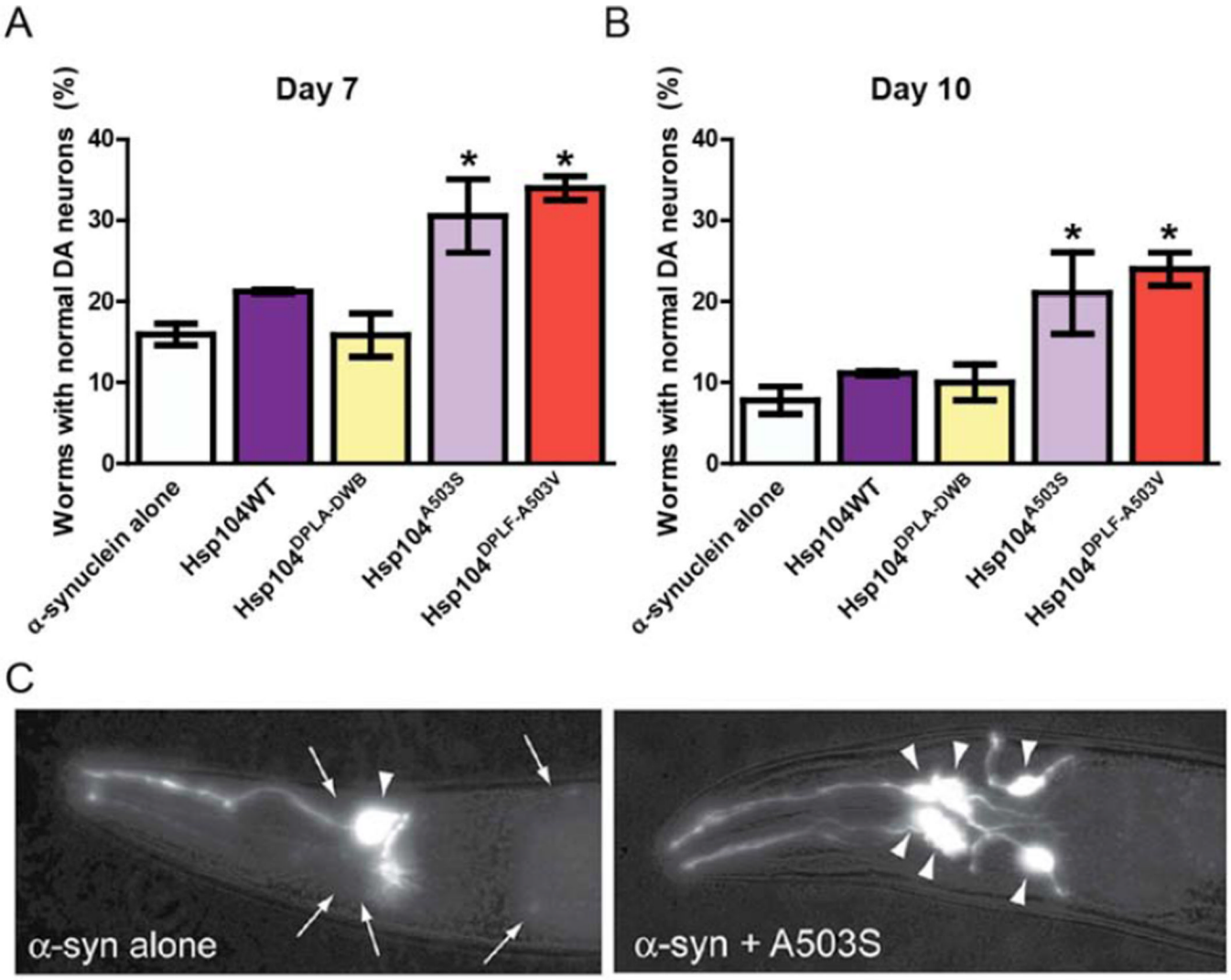

Figure 5. Hsp104^{A503S} and Hsp104$^{A503V\text{-}DPLF}$ protect against α-syn toxicity and dopaminergic neurodegeneration in *C. elegans*

(A) Hsp104 variants and α-syn were coexpressed in the dopaminergic (DA) neurons of *C. elegans*. Hermaphrodite nematodes have six anterior DA neurons, which were scored at day 7 post-hatching. Hsp104^{A503S} and Hsp104$^{A503\text{-}VDPLF}$ have significantly greater protective activity than both α-syn alone and the null variant. Normal worms have a full complement of DA neurons at this time. **(B)** At day 10, there is a decline in worms with normal DA neurons. Hsp104^{A503S} and Hsp104$^{A503V\text{-}DPLF}$ exhibit greater protective activity when compared to Hsp104^{WT} and the null variant. Values represent means±SEM (of 3 independent experiments, n=30 per replicate with 3–4 replicates per independent experiment. * p<.05 One-Way ANOVA group). Normal worms have a full complement of DA neurons at this time. **(C)** Photomicrographs of the anterior region of *C. elegans* co-expressing GFP with α-syn. Worms expressing α-syn alone (left) exhibit an age dependent loss of DA neurons. Worms expressing α-syn plus Hsp104^{A503S} (right) exhibit greater neuronal integrity. Arrows indicate degenerating or missing neurons. Triangles indicate normal neurons.

See also Fig. S5.

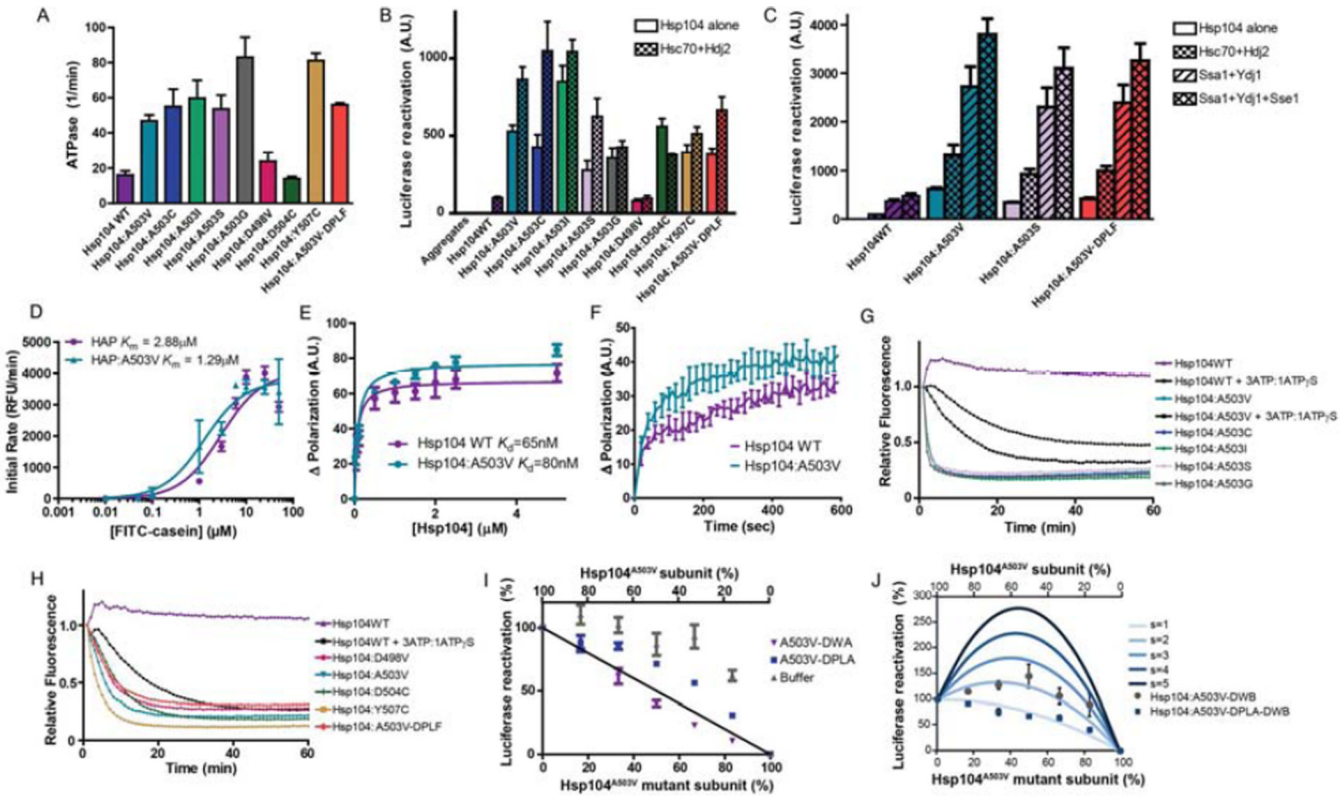

Figure 6. Potentiated Hsp104 variants are tuned differently than Hsp104^{WT}

(A) ATPase activity of Hsp104 variants. Values represent means±SEM (n=3). **(B)** Luciferase aggregates were incubated with Hsp104 variant plus (checkered bars) or minus (clear bars) Hsc70 (0.167μM) and Hdj2 (0.167μM). Values represent means±SEM (n=3) **(C)** Luciferase aggregates were incubated with Hsp104 variant plus or minus: Hsc70 (0.167μM) and Hdj2 (0.073μM); Ssa1 and Ydj1; or Ssa1, Ydj1, and Sse1. Values represent means ±SEM (n=3). **(D)** Increasing concentrations of FITC-casein were incubated with ClpP plus HAP^{WT} or HAP^{A503V}. Initial degradation rates were plotted against FITC-casein concentration to determine K_m. Values represent means±SEM (n=3). **(E)** FITC-casein was incubated with increasing concentrations of Hsp104^{WT} or Hsp104^{A503V}. Change in fluorescence polarization was plotted against Hsp104 concentration to determine K_d. Values represent means±SEM (n=3). **(F)** Kinetics of Hsp104^{WT} (1μM) or Hsp104$_{A503V}$ (1μM) binding to FITC-casein (0.1μM) assessed by fluorescence polarization. Values represent means±SEM (n=3). **(G, H)** RepA$_{1–70}$-GFP was incubated with Hsp104 variant and GroEL$_{trap}$ plus ATP or ATP:ATPγS (3:1). GFP unfolding was measured by fluorescence. Representative data are shown. **(I)** Buffer, Hsp104$^{A503V-DWA}$, or Hsp104$^{A503V-DPLA}$ was mixed in varying ratios with Hsp104^{A503V} to create heterohexamer ensembles and luciferase disaggregase activity was assessed. Values represent means±SEM (n=3). Black line denotes the theoretical curve of a probabilistic mechanism where only a single WT subunit is required for disaggregation. **(J)** Experiments were performed as in **(I)** for Hsp104$^{A503V-DWB}$ and Hsp104$^{A503VDPLA-DWB}$. Theoretical curves are shown wherein adjacent pairs of A503V:A503V or A503V:mutant subunits confer hexamer activity, while adjacent mutant subunits have no activity. Each adjacent A503V:A503V pair has an activity of 1/6. Adjacent A503V:mutant pairs have a stimulated activity (s), and the effect of various s values are depicted. Values represent means±SEM (n=3).

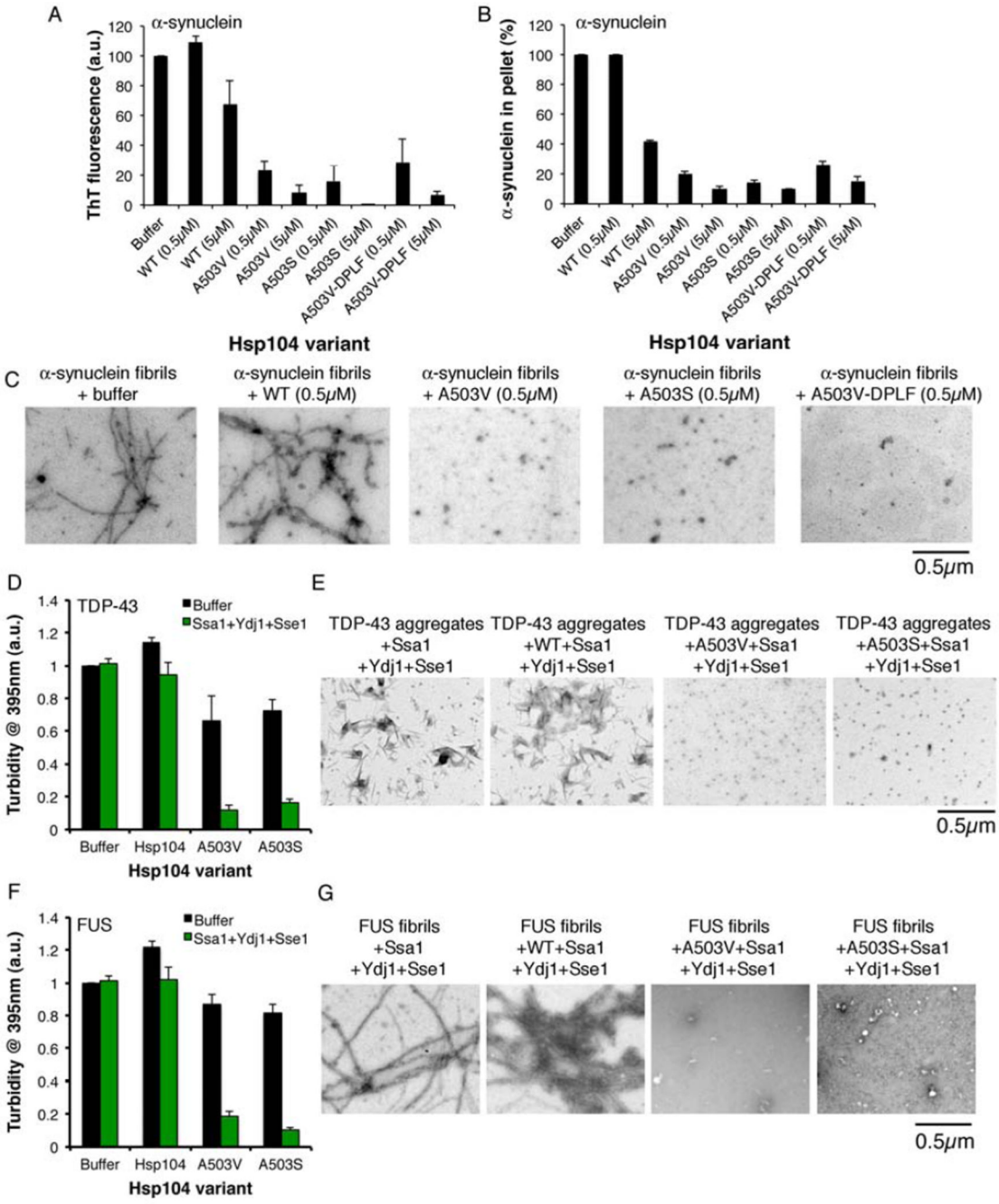

Figure 7. Potentiated Hsp104 variants disaggregate *preformed* α-syn, TDP-43, and FUS fibrils more efficaciously than Hsp104^{WT}

(A–C) α-syn fibrils were incubated without or with Hsp104^{WT}, Hsp104^{A503V}, Hsp104^{A503S}, or Hsp104$^{A503V\text{-}DPLF}$ for 1h at 30°C. Fiber disassembly was assessed by ThT fluorescence **(A),** sedimentation analysis **(B)**, or **(C)** EM (Bar, 0.5μm). **(A, B)** Values represent means±SEM (n=2). **(D, E)** TDP-43 aggregates were incubated with buffer, Hsp104^{WT}, Hsp104^{A503V}, or Hsp104^{A503S} plus or minus Ssa1, Ydj1, and Sse1 for 1h at 30°C. **(D)** Aggregate dissolution assessed by turbidity. Values represent means±SEM (n=3). **(E)** Aggregate dissolution assessed by EM. Bar, 0.5μm. **(F, G)** FUS aggregates were incubated with buffer, Hsp104^{WT}, Hsp104^{A503V}, or Hsp104^{A503S} plus or minus Ssa1, Ydj1,

and Sse1 for 1h at 30°C. **(F)** Aggregate dissolution assessed by turbidity (absorbance at 395nm). Values represent means±SEM (n=3). **(G)** Aggregate dissolution assessed by EM. Bar, 0.5μm.